Surface bidirectional reflectance and albedo properties derived using a land cover–based approach with Moderate Resolution Imaging Spectroradiometer observations

Yi Luo

Noetix Research, Inc., Ottawa, Ontario, Canada

Alexander P. Trishchenko and Rasim Latifovic

Canada Centre for Remote Sensing, Earth Sciences Sector, Natural Resources Canada, Ottawa, Ontario, Canada

Zhanqing Li

Department of Meteorology and Earth System Science Interdisciplinary Center, University of Maryland, College Park, Maryland, USA

[1] Surface bidirectional reflectance distribution function (BRDF) and albedo maps are derived from Moderate Resolution Imaging Spectroradiometer (MODIS) multiday surface reflectance composites with a 500-m spatial resolution (MODIS product MOD09A1/MYD09A1). The proposed method dubbed land cover–based fitting employs the processing of clear-sky reflectance data for similar land cover types and takes into account the magnitude of normalized difference vegetation index (NDVI). The BRDF is derived through the fitting of pixel data sorted into small bins according to the values of angular variables and NDVI. Robust statistical processing is applied to reduce the influence of noise and outliers. This method increases the success rate of the fitting process and enables more accurate monitoring of surface temporal changes during periods of rapid spring vegetation green up and autumn leaf fall, as well as changes due to agricultural practices and snow cover variations. The approach is specifically applied over the Atmospheric Radiation Measurement Program Southern Great Plains area. Results are compared to alternative BRDF/albedo products, such as the MOD43 albedo and Multiangle Imaging Spectroradiometer surface products that are derived through a pixel-based fitting process. A good agreement was generally found between different data sets. For example, the average biases in the visible and near-infrared bands are usually less than 0.01 and 0.02, respectively, and correlation coefficients are typically larger than 0.80. An analysis of these differences identifies some unique advantages of the proposed method, such as the ability to capture rapidly changing surface properties and an increased performance in the case of reduced number of clear-sky observations because of frequent cloudy conditions. Results suggest that the developed land cover–based methodology is valuable for the purpose of surface BRDF and albedo mapping using MODIS observations.

1. Introduction

[2] Surface albedo is defined as the ratio of the total (hemispheric) reflected solar radiation flux to the incident flux upon the surface. It is one of the most important parameters in atmospheric radiation studies. Albedo is important because even small changes in its magnitude can lead to variations in radiative forcing, to which climate is extremely sensitive [*Ingram et al.*, 1989; *Houghton et al.*, 2001; *Dirmeyer and Shukla*, 1994]. The spatial complexity and temporal variations of surface properties mean that practical albedo estimates over large area are usually derived from satellite observations [*Strugnell et al.*, 2001; *Cihlar et al.*, 2002; *Gutman et al.*, 1989]. Most land surfaces reflect incident radiation anisotropically. Anisotropic properties are described by the surface bidirectional reflectance distribution function (BRDF) [*Nicodemus et al.*, 1977]. An accurate determination of surface BRDF properties is essential because they are directly related to the accuracy of derived surface albedo and radiation fluxes, which are obtained as hemispheric integrals of BRDF and radiance

fields. The retrieval of surface BRDF is not a simple task since most space-borne sensors only view the ground target at limited observational geometries that are defined by the solar zenith angle (SZA), viewing zenith angle (VZA), and Sun-satellite relative azimuth angle (RAA) [*Csiszar et al.*, 2001; *Trishchenko*, 2004].

[3] There are many parametric BRDF models that are based on the physical characteristics and experimental results observed for natural surfaces [*Lucht and Roujean*, 2000]. Semiempirical linear kernel-driven models are among the most widely used of these. Kernel-driven models are attractive because of their fast operational implementation and good accuracy [*Wu et al.*, 1995; *Wanner et al.*, 1997; *Privette et al.*, 1997; *Lucht et al.*, 2000]. The derivation of BRDF parameters, i.e., the process of model inversion, is achieved through a fitting procedure that tunes the model to observed data points by minimizing mean square residuals. For a successful inversion, the observations must cover a range of Sun-target-viewer geometries (and ideally, the entire range). In practice, however, this requirement is rarely achieved. For a fixed location on the Earth's surface, some satellite systems, such as the Multi-angle Imaging Spectroradiometer (MISR), can obtain multiple angular views virtually instantaneously, while others, such as the Moderate Resolution Imaging Spectroradiometer (MODIS), build up sequential angular views over a period of time. The latter approach, hereinafter referred to as a pixel-based fitting (PBF) method, is currently implemented in the MODIS operational albedo retrieval algorithm (MOD43). It provides surface albedo for each 1-km pixel at 16-day intervals [*Schaaf et al.*, 2002]. This 16-day sampling period is deemed to be long enough to acquire a number of clear-sky observations over a range of Sun-target-viewer geometries. However, a shorter sampling period may be required by applications where surface properties vary rapidly over short timescales (e.g., during periods of snow fall, snowmelt, and soil moisture and vegetation change). In such cases, the shortening of the time interval in the PBF approach reduces the number of clear-sky data points used in the fitting procedure. This makes the retrieval of albedo less reliable or may result in a failure of the inversion procedure. Even for a 16-day sampling interval and for a maximal potential number of clear-sky data points included in the inversion procedure, the retrievals may still fail or produce biased results because of intrinsic noise in the data [*Jin et al.*, 2003a]. *Moody et al.* [2004] demonstrated that there is a pressing need to improve the spatial completeness of the MODIS operational albedo product because of significant gaps in the data. About 50% of useful data are of lower quality or missing on a global scale because of insufficient sampling of clear-sky pixels for BRDF/albedo retrievals.

[4] A land cover–based fitting (LBF) approach is presented in this paper. This method reduces the difficulties associated with a small number of data points in the fitting procedure, and produces BRDF/albedo products for shorter time intervals. Our approach employs the similarity in the BRDF properties of various pixels, if these pixels belong to the same land cover type, are in a similar biophysical condition, and occur within the same climatic region [*Trishchenko et al.*, 2004; *Latifovic et al.*, 2003]. For any given region of interest, clear-sky pixels and land cover information are used to derive BRDF model parameters for each land cover type in the region. The LBF approach overcomes the limitations of PBF approaches that are associated with a small or insufficient amount of data used in the fitting process. It does this by (1) providing improved sampling in terms of the number of observations and range of geometries used and (2) requiring less computational resources than other approaches. The LBF method can be implemented for shorter time intervals, enabling the capture of a rapid change in BRDF characteristics. The potential limitation of this approach is a reduced sensitivity to subtle spatial differences in BRDF shape within the same land cover class.

[5] This paper describes and applies the LBF methodology to the MODIS surface reflectance product (MOD09A1 for Terra and MYD09A1 for Aqua) (E. F. Vermote and A. Vermeulen, Atmospheric correction algorithm: Spectral reflectances (MOD09), in *MODIS Algorithm Technical Background Document*, NASA report, contract NAS5-96062, 1999, available at http://modis.gsfc.nasa.gov/data/atbd/atbd_mod08.pdf, hereinafter referred to as Vermote and Vermeulen, 1999). The MOD09A1/MYD09A1 product contains the MODIS surface reflectance composite data generated at a 500-m spatial resolution and at 8-day intervals. This product also includes angular variables, such as SZA, VZA, and RAA, as well as the date of observation, quality flags and a variety of auxiliary information (http://edcdaac.usgs.gov/modis/mod09a1v4.html). The LBF methodology is tested over the Southern Great Plains (SGP) region. This region is in the focus of the Atmospheric Radiation Measurement (ARM) program (http://www.arm.gov). The ARM SGP site serves as an important test bed for the physics of climate and climate change research, atmospheric radiation budget and weather/climate models [*Ackerman and Stokes*, 2003]. Spatially and temporally complete high-quality surface BRDF/albedo maps of this area will greatly assist the ARM program to achieve its major objective "to improve understanding of the processes and properties that affect atmospheric radiation" [*Stokes and Schwartz*, 1994]. The understanding and modeling of atmospheric radiation and cloud processes may be improved in climate and weather prediction studies by taking into account realistic albedo variations with solar zenith angle, land cover type, and seasonal vegetation phenology [*Lucht and Roujean*, 2000].

[6] The structure of this paper is as follows: The general methodology and its realization are described in section 2. This includes the basic concept of the BRDF LBF methodology, data description, BRDF model specification, and implementation procedure. Section 3 analyses some typical BRDF results for the ARM SGP area. Comparisons of LBF BRDF/albedo data with other products, such as MODIS MOD43B1and MISR albedo, are presented in section 4. Section 5 contains conclusions and final discussion.

2. BRDF Land Cover–Based Fitting (LBF) Methodology

2.1. Basic Concept

[7] Surface BRDF is physically determined by the geometric structure of the land surface as well as the optical

properties of canopy elements, understory, and soil conditions. Several parametric BRDF models have been developed based on various assumptions about these properties [e.g., *Roujean et al.*, 1992; *Li and Strahler*, 1992; *Rahman et al.*, 1993]. Surface structure influences the BRDF through the reflectors' geometric features, their shadow casting and their spatial distribution. Optical characteristics account for the absorbing and scattering effects that the surface elements exert on the radiation field. The BRDF model parameters are closely related to land cover type [e.g., *Wu et al.*, 1995; *Lucht et al.*, 2000]. As shown by *Trishchenko et al.* [2004] and *Latifovic et al.* [2003], it is reasonable to assume that the BRDF shape is generally similar for the same land cover type under similar biophysical conditions characterized by the normalized difference vegetation index (NDVI).

[8] The LBF approach uses a multiday clear-sky composite of surface reflectance and groups pixels by land cover type and NDVI value. Landcover and NDVI data are both required for the successful implementation of the LBF approach. Grouped data are then used to optimally fit the BRDF model parameters for each land cover type. After these generic BRDFs are obtained, pixel-level BRDFs are determined by adjusting the general land cover BRDF to the observed reflectances of a given pixel. A similar strategy was successfully employed for BRDF/albedo retrievals from advanced very high resolution radiometer (AVHRR) and SPOT-VEGETATION data [*Cihlar et al.*, 2002, 2004; *Latifovic et al.*, 2003, 2004; *Li et al.*, 1996].

2.2. Land Cover Map Over the ARM SGP Area

[9] The National Land Cover Data Set (NLCD) is used in this study. The NLCD was compiled from Landsat Thematic Mapper (TM) satellite imagery at 30-m spatial resolution and supplemented by various ancillary data. It was produced as part of a cooperative project between the U.S. Geological Survey (USGS) and the U.S. Environmental Protection Agency (USEPA) (http://landcover.usgs.gov/natllandcover.asp). The original NLCD land cover data set was resampled to create a land cover map that matched the spatial resolution of the MODIS data used in this study (500 m). Each land cover class in the resampled data set was then converted to its International Geosphere-Biosphere Programme (IGBP) equivalent following the approach described by *Latifovic et al.* [2004]. The IGBP classification was selected because of its frequent use in climate modeling and ecological studies. The preference was given to the NLCD land cover map rather than the MODIS land cover product (MOD12) (A. Strahler et al., MODIS land cover product: Algorithm theoretical basis document (ATBD) version 5.0, 1999, available at http://modis.gsfc.nasa.gov/data/atbd/atbd_mod12.pdf) because the latter is only available at a spatial resolution of 1 km, and because the use of the former avoids potential biases and correlation impacts between products from the same sensor.

[10] The study region covers an 8° latitude × 10° longitude area centered at the ARM SGP Central Facility (CF) located in northern Oklahoma, United States. Figure 1 shows the spatial distribution of the 10 IGBP land cover classes that occur in the region. The area is dominated by grasslands (53%), croplands (19%) and deciduous forest (13%).
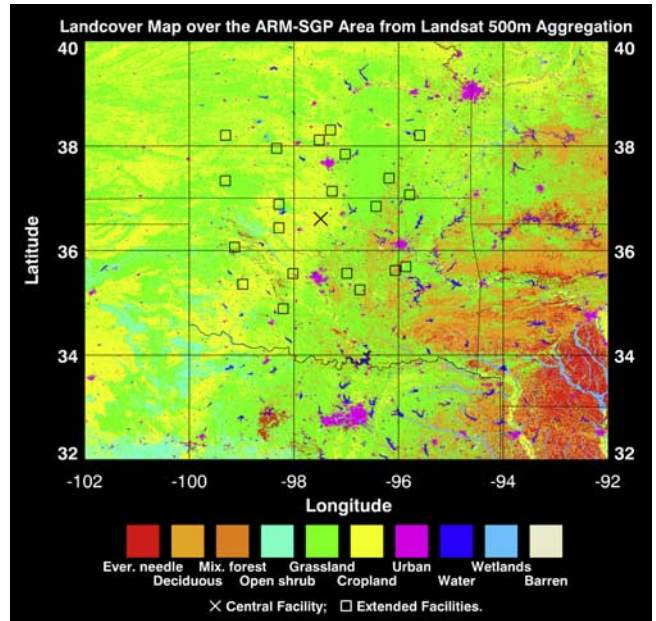

Figure 1. Land cover map in the International Geosphere-Biosphere Programme legend for the Atmospheric Radiation Measurement (ARM) Southern Great Plains (SGP) area (north Oklahoma, United States). There are total 10 land cover types identified in this area. The cross at the center indicates the location of the ARM central facility (CF), and the squares mark the extended facilities locations.

Less frequent land cover types include evergreen forest (3.9%) and open shrublands (3.5%). While cropland is the main land cover type around the CF, it is mixed with grasslands in the western and northern parts of the study area. In addition, shrublands are present in the southwest part of the study area, while the southeasternmost portion of the study area is dominated by forest. Usually, the dominant land cover types are geographically concentrated over relatively uniform area.

2.3. BRDF Shape and NDVI

[11] The BRDF of the land surface is dependent on both land cover (vegetation) type and vegetation condition [e.g., *Wu et al.*, 1995; *Li et al.*, 1996]. The vegetation condition can be described by the magnitude of the NDVI [*Gutman*, 1987]. Data collected from fine-resolution Landsat imagery and the MISR 1-km surface product illustrate the impact of NDVI on BRDF. Figure 2a shows a Landsat-7 Enhanced Thematic Mapper (ETM) image acquired over the ARM SGP CF area on March 9 (day 68) 2002. The image contains a mixture of cropland and grassland (pasture) according to field surveys for that area [*Li et al.*, 2002]. Analysis uses MISR observations over a 2 × 2 km^2 area of cropland close to the CF (marked as square in Figure 2a) to illustrate the variability in surface BRDF properties with NDVI. The MISR sensor is well suited for such an analysis because it views the target at nine angles almost instantaneously with a footprint size of 1.1 km [*Diner et al.*, 1998]. The MISR spatial resolution is, however, somewhat too coarse to resolve the spatial variation of the BRDF inherent to various crop types. This may reduce
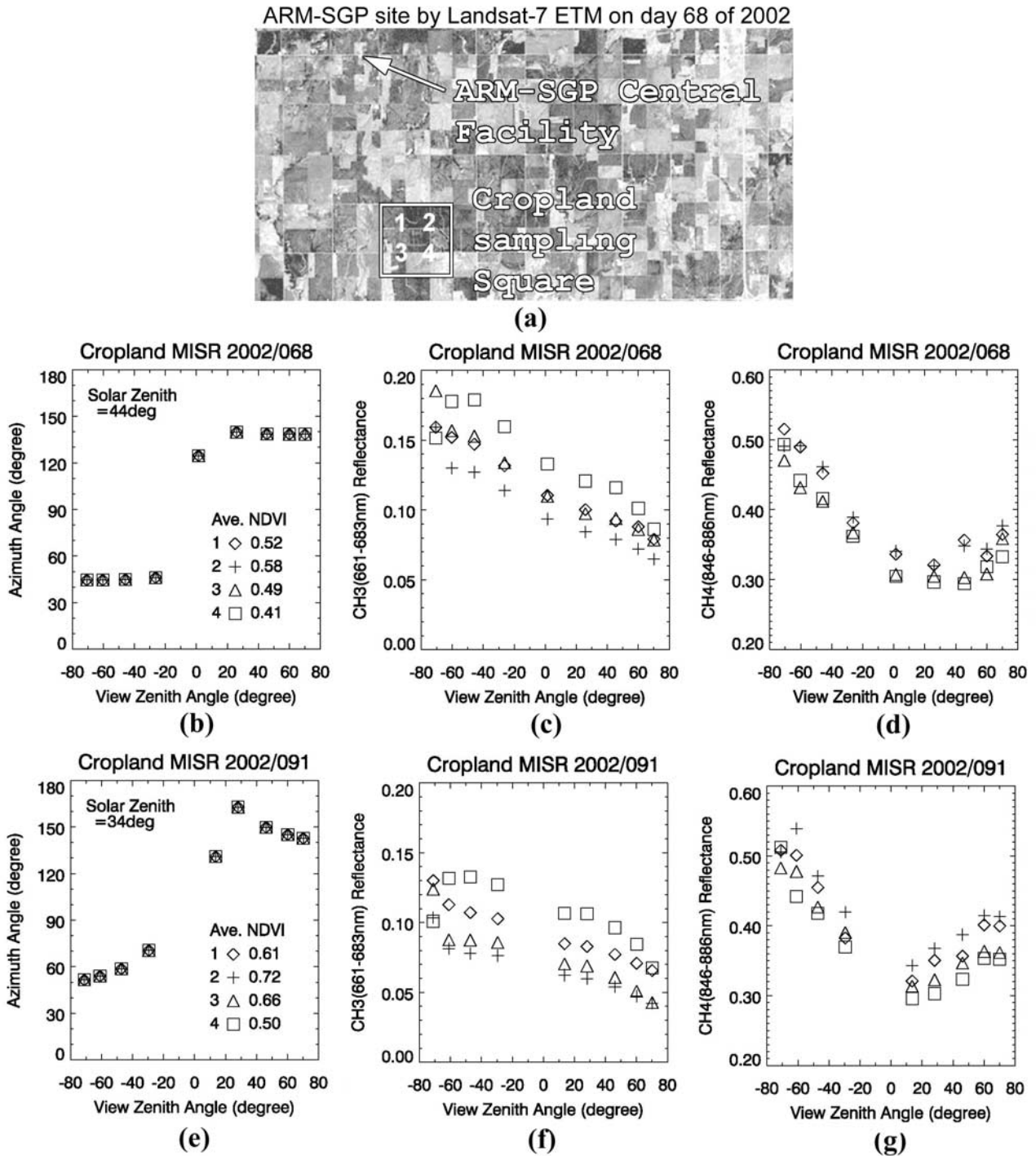
Figure 2. (a) View of the ARM SGP CF area from the Landsat-7 Enhanced Thematic Mapper (ETM) on day 68 (9 March) 2002. The cropland sampling square corresponds roughly to a 2.2 × 2.2 km area (2 × 2 Multiangle Imaging Spectroradiometer (MISR) pixels). (b) Relationship between relative azimuth angle (RAA) and viewing zenith angle (VZA) and normalized difference vegetation index (NDVI) from MISR observations on day 68 of 2002 for the cropland sampling square. (c) Relationship between surface reflectances and VZA in the red band on day 68 of 2002. (d) Relationship between surface reflectances and VZA in the NIR band on day 68 of 2002. (e) Relationship between RAA and VZA and NDVI from MISR observations on day 91 of 2002 for the cropland sampling square. (f) Relationship between surface reflectances and VZA in the red band on day 91 of 2002. (g) Relationship between surface reflectances and VZA in the NIR band on day 91 of 2002. Diamonds, crosses, triangles, and squares denote the data for the 2 × 2 pixels in the MISR scan shown in Figure 2a.

the actual contrast between various BRDFs. The selected sampling area corresponds to a group of 2×2 pixels in the MISR data. The observations for each pixel are also shown in Figure 2 as a function of the RAA versus VZA (Figure 2b), surface reflectance versus VZA for the red band (661–683 nm) (Figure 2c) and surface reflectance versus VZA for the near-infrared (NIR) band (846–886 nm) (Figure 2d). The averaged NDVI values (within $\pm 50°$ VZA) are also given in Figure 2b. Figures 2b–2d show the MISR reflectances for the same day as that of the Landsat image. Figures 2e–2g show the MISR reflectances 3 weeks later (1 April (day 91) 2002). The SZAs for day 68 and 91 are approximately $44°$ and $34°$, respectively. Figure 2 shows that the magnitude of NDVI defines the BRDF shape in a unique way. For day 68, pixels 1 and 3 have similar NDVI and reflectances values. Pixels 2 and 4, however, have an NDVI difference of nearly 0.2, which corresponds to the large difference in vegetation density seen in Figure 2a. The reflectances and BRDF profiles of these pixels are thus substantiality different, especially in the red band. Specifically, the red band reflectance for pixel 4 is strongest for the back-scattered viewing geometry when the VZA is close to the SZA. It should also be noted that the temporal trend in the surface properties, even after only 3 weeks, is considerable. This reflects a rapid change in vegetation properties during the peak of the growing season as confirmed by the magnitudes of NDVI between these dates. This emphasizes the advantage of having shorter sampling intervals than the 16-day period currently adopted in the operational MODIS BRDF/albedo processing. A shorter sampling interval is especially important during periods when surface properties change rapidly or when detailed knowledge of phenological change is required.

2.4. RossThick–LiSparse Reciprocal BRDF Model

[12] The RossThick–LiSparse model (hereinafter referred to as Ross-Li) is employed in this study. The Ross-Li model has been identified as one of the most appropriate models for the operational processing of MODIS data [*Wanner et al.*, 1997; *Privette et al.*, 1997; *Li et al.*, 1997; *Lucht and Lewis*, 2000]. It has also been demonstrated that the Ross-Li and the nonlinear Rahman's models [*Rahman et al.*, 1993; *Martonchik*, 1997] perform similarly. However, the linear Ross-Li model is more computationally efficient.

[13] The linear BRDF model is expressed as a sum of several theoretically constructed kernel functions f_i (θ_s, θ_v, ϕ), where θ_s, θ_v and ϕ are the SZA, VZA and RAA, respectively. The reciprocal model of Ross-Li [*Wanner et al.*, 1995] is a model that uses three kernels

$$\rho_\lambda(\theta_s, \theta_v, \phi) = a_0 + a_1 f_1(\theta_s, \theta_v, \phi) + a_2 f_2(\theta_s, \theta_v, \phi), \quad (1)$$

where f_1 is the RossThick kernel and represents volumetric scattering from a dense leaf canopy based on a single-scattering approximation of radiative transfer theory [*Ross*, 1981; *Roujean et al.*, 1992] and f_2 is the LiSparse kernel which is derived from the geometric-optical mutual shadowing model and assumes a sparse ensemble of surface objects [*Li and Strahler*, 1992]. Parameters a_0, a_1 and a_2 are coefficients of the kernels and are related to the isotropic,

volumetric and geometric components, respectively. Kernels are given by the following expressions:

$$f_1 = [(\pi/2 - \xi)\cos\xi + \sin\xi]/[\cos\theta_s + \cos\theta_v] - \pi/4, \quad (2)$$

where $\cos\xi = \cos\theta_s \cos\theta_v + \sin\theta_s \sin\theta_v \cos\phi$

$$f_2 = O(\theta_s, \theta_v, \phi) - \sec\theta_s' - \sec\theta_v' + \frac{1}{2}(1 + \cos\xi')\sec\theta_s'\sec\theta_v'. \quad (3)$$

$$O = \frac{1}{\pi}(t - \sin t \cos t)(\sec\theta_s' + \sec\theta_v')$$

$$\cos t = \frac{h}{b}\frac{\sqrt{D^2 + (\tan\theta_s'\tan\theta_v'\sin\phi)^2}}{\sec\theta_s' + \sec\theta_v'}$$

$$D = \sqrt{\tan^2\theta_s' + \tan^2\theta_v' - 2\tan\theta_s'\tan\theta_v'\cos\phi}$$

$$\cos\xi' = \cos\theta_s'\cos\theta_v' + \sin\theta_s'\sin\theta_v'\cos\phi$$

$$\theta_v' = \tan^{-1}\left(\frac{b}{r}\tan\theta_v\right); \quad \theta_s' = \tan^{-1}\left(\frac{b}{r}\tan\theta_s\right);$$

the two ratios, h/b and b/r, describe the relative height and shape of crown. In this paper, we used values of $h/b = 2$ and $b/r = 1$, as recommended by *Lucht et al.* [2000].

2.5. Procedure Implementation

[14] The implementation of proposed LBF method for derivation of surface BRDF parameters involves several steps:

[15] 1. Input data are taken from the MOD09A1 product (version 4) for MODIS on Terra satellite and MYD09A1 for MODIS on Aqua satellite. These are MODIS atmospherically corrected surface clear-sky reflectances composited over 8-day intervals with a spatial resolution of 500 m (see http://edcdaac.usgs.gov/modis/mod09a1v4.html). The MOD09A1/MYD09A1 archive contains seven spectral bands from 0.46 to 2.15 μm. Bands are located in the shortwave domain and designed for land monitoring applications. Data are calibrated to an absolute scale using the MODIS on-board calibration technique and are accurately geolocated. The data set also includes snow and ephemeral water flags. Cloud screening and atmospheric corrections are carried out using the synchronous onboard observations available from the ensemble of MODIS channels and MODIS data processing technology (Vermote and Vermeulen, 1999).

[16] 2. The MOD09A1/MYD09A1 data are remapped using MODIS reprojection tool (see http://edcdaac.usgs.gov/landdaac/tools/modis/index.asp) from the native Sinusoidal (SIN) grid onto a latitude-longitude projection over the ARM-SGP $8° \times 10°$ area. A pixel size of 500 m was maintained during the reprojection procedure. To maintain compatibility with other widely used data sets, the data are then rearranged from an 8-day composite interval to a 10-day composite interval. This procedure is possible because the MOD09A1/MYD09A1 data contain information on the data acquisition date of each pixel.

[17] 3. All pixels in the study area are grouped according to land cover type. To reduce noise, pixels marked as bad
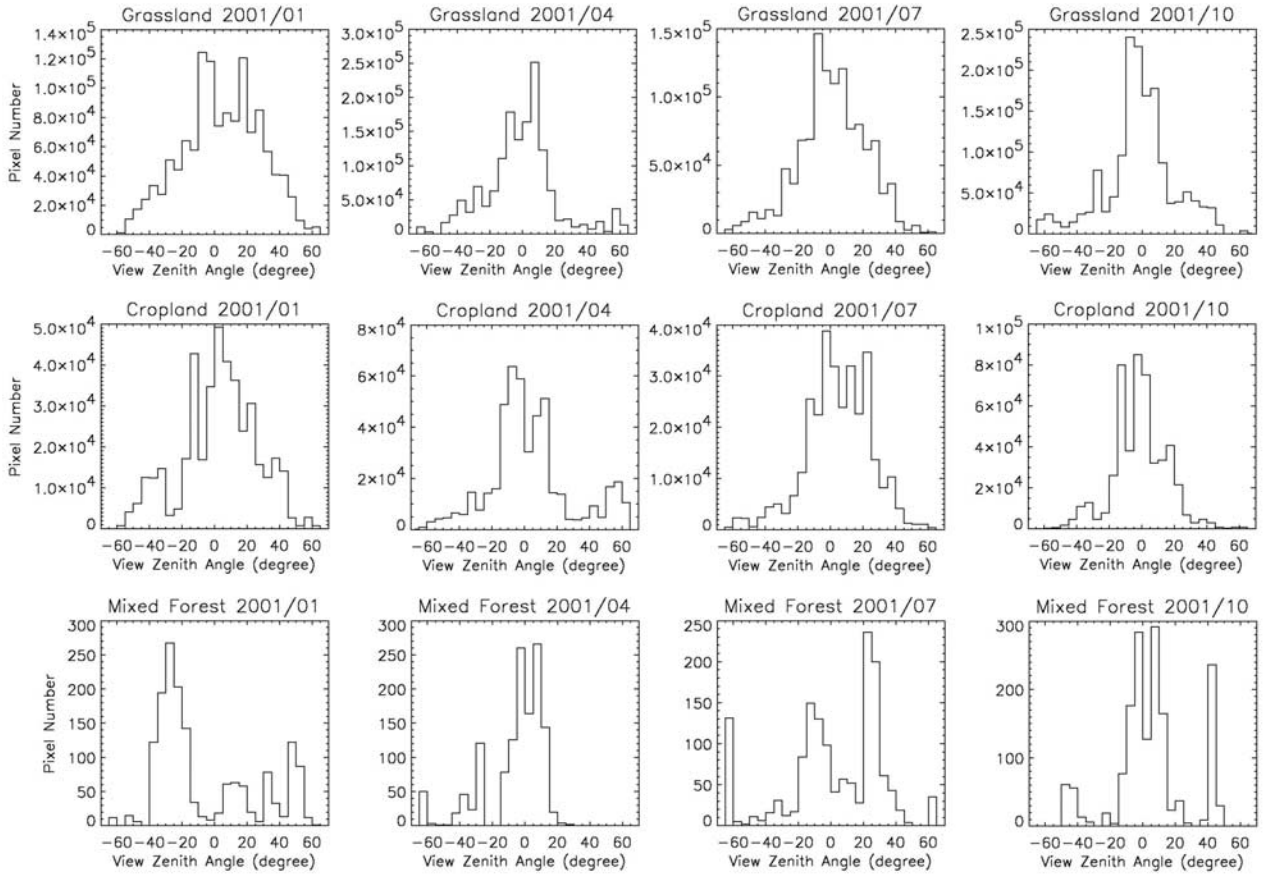
Figure 3. Histograms of the VZA from Moderate Resolution Imaging Spectroradiometer (MODIS) observations for (top to bottom) grasslands, croplands, and mixed forest in (left to right) January, April, July, and October of 2001 in the ARM SGP area.

quality or contaminated by clouds are excluded from the analysis. Pixels that contain some portion of snow cover are selected for separate processing. Snow pixels can be identified by their high reflectance in the visible band and relatively low reflectance in the shortwave infrared band. The normalized difference snow index (NDSI) or operational snow cover products can be used to identify and remove snow effects in surface reflectance [*Hall et al.*, 2002].

[18] 4. The land cover–grouped data are further grouped into smaller bins according to their NDVI levels and values of angular variables. Data binning according to angular values is required to lessen the impact of the irregular distribution of the observational geometry. The histograms of VZA presented in Figure 3 show the distribution of sampling geometries for several land cover types and seasons. The distribution of angles depends on several factors, such as the orbit configuration, the sensor scanning mode, the distribution of the clear-sky area, and the spatial patterns of land cover. The distribution of VZA and RAA is generally nonuniform. If the data are directly used in the fitting process, unequal weights at different angles may bias the fitting results toward data with the most frequently observed geometries. This causes the equally important but less frequent data points to have little influence on the retrieved BRDF model. To address this problem, all data points for each land cover class are sorted into data bins

defined by certain NDVI and angular intervals, and only one value from each data bin contributes to the fitting process. In this paper intervals for the NDVI, and the SZA, VZA and RAA, are 0.1, and 5°, 5° and 10°, respectively.

[19] 5. Before the fitting procedure is initiated, the data collected in each data bin are statistically preprocessed. A robust statistical procedure resistant to outliers similar to that proposed by *Trishchenko* [2002] is employed. The procedure sorts all data according to their values, removes the lowest and highest 5% points of the sample and then computes the average. Only one value is derived for each bin after applying the statistical procedure. This value represents the observed reflectance and geometry for that data bin. Examples of bin-processed data for grasslands are given in Figure 4 (SZA is not grouped here). Figure 4 also shows the polar plots of MODIS surface reflectance in two spectral bands (red and NIR) for 4 months over the ARM SGP study area. The average SZA value and its range are given at the top of each panel. The radius of the polar plot represents the VZA, and the polar angle corresponds to the RAA. The polar plots clearly show how the azimuth angle varies with season. This angle is close to the perpendicular plane (90°/270°) in winter and autumn (Figures 4a and 4d), and closer to the principal plane (0°/180°) in summer (Figure 4c). The BRDF shape generally shows larger reflectances in the backscattering direction, when the RAA is close to the principal plane. This is consistent with
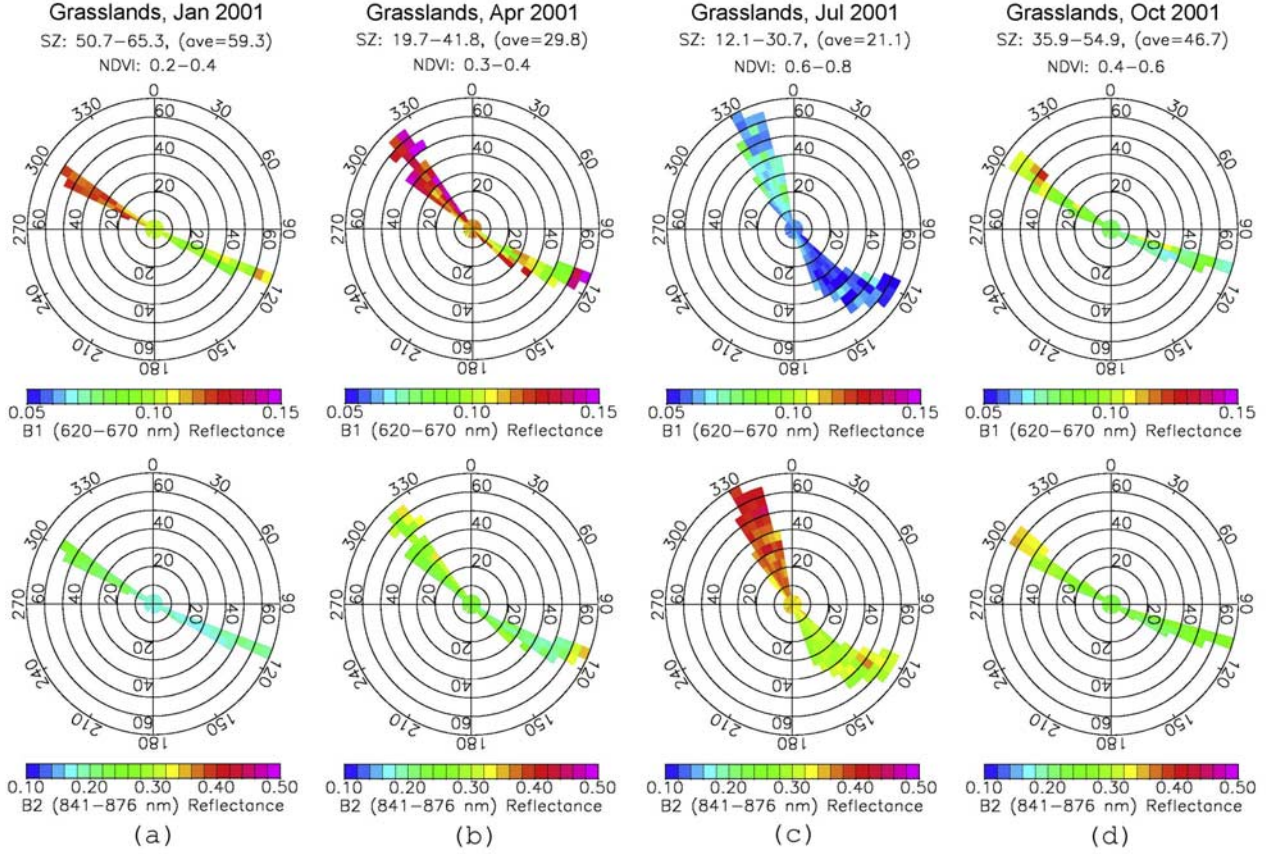
Figure 4. Polar plots of the surface reflectance from MODIS observations for two spectral bands ((top) red and (bottom) near-infrared (NIR)) for grasslands in the ARM SGP area: (a) January 2001, (b) April 2001, (c) July 2001, (d) October 2001. The SZA range, its average for each month, and NDVI intervals are indicated at the top of each panel. The radius of the polar plot represents the VZA, while the polar angle represents the RAA.

the commonly observed hot spot effect [*Kuusk*, 1991]. It is important to note the narrow range of RAA, which is a major source of uncertainty in determining the BRDF function for the entire range of three variables (SZA, VZA, and RAA).

[20] 6. The land cover–grouped and preprocessed data are used to determine a set of optimal parameters for the Ross-Li BRDF model (equation (1)). In this paper, the nonlinear least squares method of Levenberg-Marquardt [*Press et al.*, 1992] is employed for the fitting process.

[21] 7. Pixel-level BRDF parameters are retrieved by scaling the land cover- and NDVI-dependent BRDF parameters obtained in step 6 to the observations at each pixel according to equation (4):

$$\rho_\lambda(\theta_s, \theta_v, \phi) = \left[1 + \frac{a_1}{a_0} f_1(\theta_s, \theta_v, \phi) + \frac{a_2}{a_0} f_2(\theta_s, \theta_v, \phi) \right]$$
$$\cdot \frac{\rho_\lambda^{obs}(\overline{\theta}_s, \overline{\theta}_v, \overline{\phi})}{\left[1 + \frac{a_1}{a_0} f_1(\overline{\theta}_s, \overline{\theta}_v, \overline{\phi}) + \frac{a_2}{a_0} f_2(\overline{\theta}_s, \overline{\theta}_v, \overline{\phi}) \right]}, \quad (4)$$

where $\overline{\theta}_s$, $\overline{\theta}_v$, $\overline{\phi}$ are angles corresponding to the geometry of observed clear-sky pixel.

[22] When the observed data for some pixels are cloud-contaminated or are of bad quality, an interpolation is performed based on the model results (derived from clear-sky data elsewhere in the region) and multiyear statistics for a particular pixel and time interval. The pixel-level BRDF parameters are temporally interpolated and smoothed if further data gaps or outliers are identified. This process uses a complete phenological cycle (12 months) of time series data for each pixel, and employs a Fourier transform filter technique.

[23] 8. The hemispheric reflectance, i.e., albedo, is computed using the BRDF parameters. Two types of albedo are distinguished: direct and diffuse [*Iqball*, 1983]. Direct albedo is defined as the albedo of the surface illuminated by a direct beam of radiation. Diffuse albedo is defined as the albedo of the surface under a fully isotropic downward radiance field. With a linear model like the Ross-Li, both types of albedo can be computed using a lookup table of precomputed kernel integrals or by using analytical approximations that express albedo as a function of BRDF parameters and SZA [*Lucht et al.*, 2000; *Schaaf et al.*, 2002]. The albedo of the surface under natural illumination, i.e., the superposition of direct and diffuse radiance fields, can be estimated as a linear combination
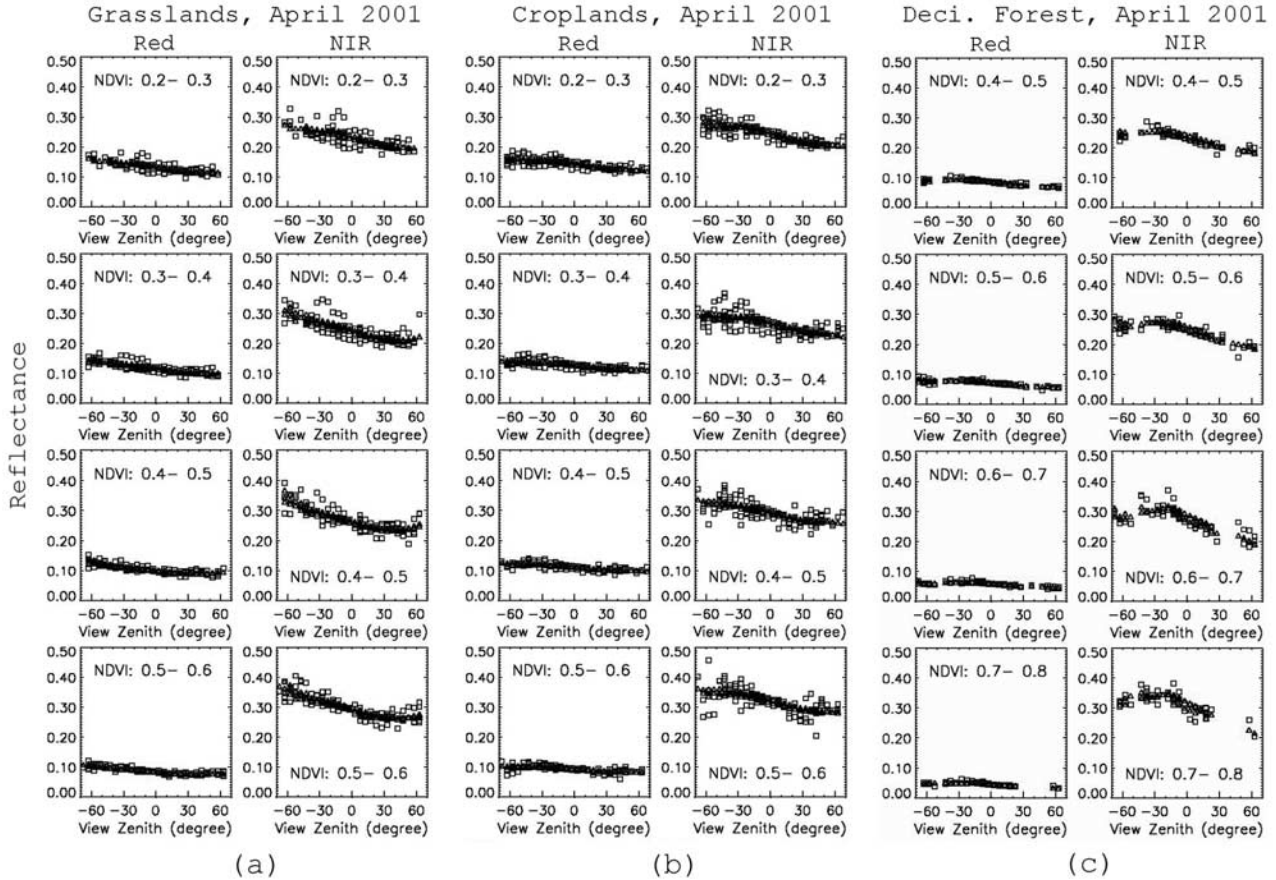
Figure 5. MODIS reflectances at the red and NIR bands plotted against the VZA for different NDVI intervals in April 2001 for (a) grassland, (b) cropland, and (c) deciduous forest. The squares correspond to the observed values from each preprocessed data bin (obtained in step 5, see text for details). The triangles correspond to the results of fitting the RossThick–LiSparse bidirectional reflectance distribution function (BRDF) model as described in the text.

of direct and diffuse albedo components, with the weights depending on the atmospheric conditions.

3. BRDF and Albedo Results

[24] The results of fitting MODIS reflectances by the Ross-Li model using the LBF methodology are shown in Figure 5. The reflectances in the red and NIR bands are plotted against the VZA for grasslands (Figure 5a), croplands (Figure 5b), and deciduous forest (Figure 5c) at various NDVI levels for April 2001. As expected, these plots show that observations are sampled almost continuously against the VZA axis and with approximately equal weights. The observations cover a wide range of viewing geometries and clearly produce an anisotropic BRDF shape. The observations and model fitting results are distributed as tight clusters. This indicates that successful fittings have been mostly achieved. The BRDF dependence upon NDVI is smooth within each land cover type. The magnitude of a BRDF varies much more than its shape, which provides an additional support to the LBF methodology. On the other hand, the differences in the BRDF shape among the land cover types are obvious. For example, grasslands (Figure 5a) always show relatively smaller forward scattering (i.e.,

when VZA > 0) and much smoother backward scattering reflectances (i.e., when VZA < 0) compared to cropland (Figure 5b). This is probably due to the smaller size of grass leaves and larger and more uniform volume density of grasslands [*Wu et al.*, 1995]. In the case of forests (Figure 5c), a distinct reflectance peak in the backscattering direction is observed. This is caused by their large protruding canopy shape. The same argument may be made from Figure 6, which conveys similar information to that shown in Figure 5 but for July 2001. Here the fitting results for grasslands (Figure 6a) and croplands (Figure 6b) are close, indicating similarity of their properties in summertime. The BRDF shapes for croplands (Figure 6b) and forest (Figure 6c) in July are considerably different from those in April (Figures 5b and 5c). This partially reflects the fact that the canopy for the croplands and forest changes differently between the summer and spring.

[25] The retrieved parameters of the Ross-Li BRDF model for four major land cover types in April 2001 at different NDVI levels are presented in Tables 1 and 2 for the red and NIR bands, respectively. The relative errors (standard deviations normalized by the mean), which indicate the agreement between the model fit and observations, are also listed. Most errors are less than 10%,
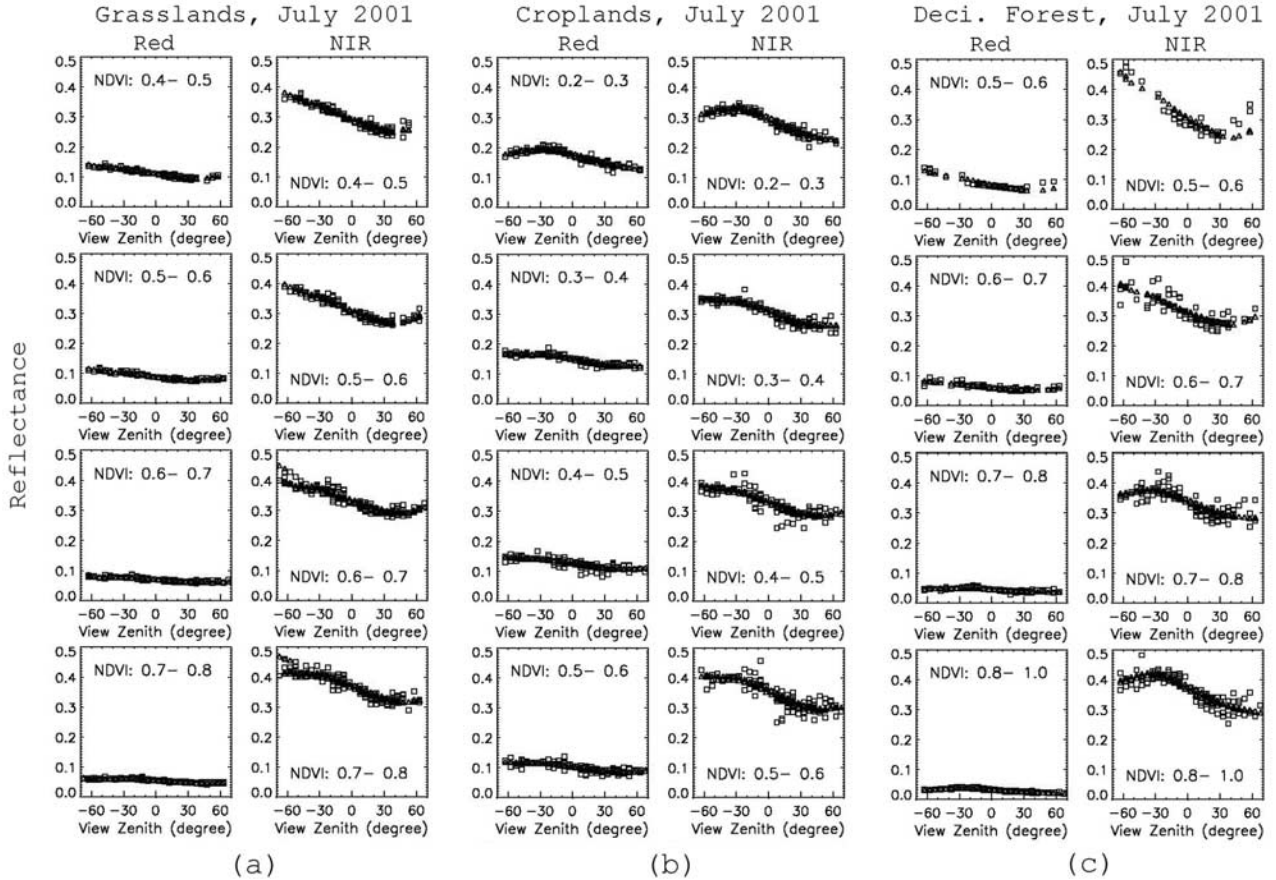
Figure 6. MODIS reflectances for the red and NIR bands plotted against the VZA for different NDVI intervals in July 2001 for (a) grassland, (b) cropland, and (c) deciduous forest. The squares correspond to the observed values from each preprocessed data bin. The triangles correspond to the results of fitting the RossThick–LiSparse BRDF model.

which indicates successful fitting. On the other hand, one may notice a deficiency in fitting the BRDF for the NIR reflectance over cropland (Figure 5b) whose data points show apparent hot spots, but the fitting curves tend to miss them. This may originate from the limitation of the kernel functions [*Chen and Cihlar*, 1997].

[26] For theoretical modeling kernels, the parameters a_0, a_1 and a_2 are considered as functions of the surface structural properties, the optical properties of canopy elements and the leaf area index (LAI) [*Wanner et al.*, 1995]. If it is assumed that the canopy structure and optical properties are defined by land cover type, then for a given land cover type the parameters a_0, a_1 and a_2 should only be a function of LAI, which is highly correlated to NDVI [*Wu et al.*, 1995; *Li et al.*, 1996; *Knyazikhin et al.*, 1998]. Because two kernels in the Ross-Li model diminish to zero when $\theta_v = 0$ and $\theta_s = 0$, parameter $a_0 = \rho_\lambda (0, 0, \phi)$, which is the bidirectional reflectance at nadir view and overhead Sun.

[27] Tables 1 and 2 show that when NDVI increases, the value of a_0 for all land cover types monotonically decreases in the red band but increases in the NIR band. This is a typical feature of reflectance for vegetated surfaces. However, other parameters do not always display such a simple relationship with NDVI. For example, while the volumetric scattering parameter a_1 decreases for the red band and

increases for the NIR band for shrublands, the geometric parameter a_2 decreases for both bands. This may imply that shrublands become denser and more uniform as NDVI increases. As a result, volumetric scattering is weakened in the red band because of a higher absorption by denser leaves. It is more intensive in the NIR band because of the greater reflection by denser leaves. The geometric scattering, caused by shadowing effects, becomes less significant with increasing NDVI. However, in the case of the forested land cover types, geometric scattering becomes more significant, and a_2 increases with NDVI, especially in the NIR band. The isotropic scatterings (a_0) of grassland and cropland are similar at different NDVI levels (although the values for croplands are slightly larger), the volumetric scattering of grasslands is larger than that of croplands, and the geometric scattering of grasslands is generally smaller than croplands. The latter finding probably occurs because grass leaves are smaller in size and denser in volume than croplands.

[28] Negative values of a_1 or a_2 may appear occasionally during unconstrained inversion processes and usually when these parameters are very small. Such values correspond to unphysical behavior of the model kernels [*Lucht and Roujean*, 2000]. This may occur because of noise in the data and/or insufficient angular samplings. Another possible reason is the lack of orthogonality

Table 1. RossThick−LiSparse BRDF Parameters for the Red Band (April 2001)[a]

NDVI	0.1−0.2	0.2−0.3	0.3−0.4	0.4−0.5	0.5−0.6	0.6−0.7	0.7−0.8	0.8−1.0
				Open Shrublands				
a_0	-	0.171	0.142	0.118	0.097	0.076	0.056	0.042
a_1	-	0.128	0.120	0.122	0.086	0.042	0.025	0.020
a_2	-	0.028	0.026	0.019	0.017	0.009	0.004	0.003
Error, %	-	11.65	11.38	11.52	8.41	7.25	7.03	5.62
				Grasslands				
a_0	-	0.150	0.131	0.107	0.091	0.075	0.057	0.043
a_1	-	0.121	0.114	0.112	0.079	0.024	0.027	0.032
a_2	-	0.017	0.015	0.005	0.006	0.006	0.003	0.003
Error, %	-	9.43	9.59	8.13	6.93	9.20	7.60	7.17
				Croplands				
a_0	-	0.162	0.140	0.122	0.104	0.083	0.061	0.041
a_1	-	0.070	0.054	0.056	0.044	0.034	0.040	0.023
a_2	-	0.021	0.015	0.012	0.012	0.009	0.003	0.001
Error, %	-	8.07	8.09	7.74	9.86	10.03	11.40	11.58
				Deciduous Forest				
a_0	-	-	0.111	0.101	0.085	0.070	0.055	0.042
a_1	-	-	0.063	0.032	0.035	0.016	0.021	0.018
a_2	-	-	0.011	0.018	0.017	0.014	0.013	0.012
Error, %	-	-	11.92	5.80	6.84	7.55	8.92	3.94

[a]Variables a_0, a_1, and a_2 represent isotropic, volumetric, and geometric parameters, respectively.

between the model kernels. Negative values for one parameter can be compensated by other parameters to make the overall results well fitted to the observations. In our case, when a negative solution occurs for a parameter, it is set to zero and the fitting process for other parameters is repeated.

[29] Figure 7 shows the BRDF effects over the entire viewing domain, as provided by a model fit for the observations previously illustrated in Figure 4. The magnitude and pattern of BRDF vary with season, which reflects the change of surface properties and Sun-sensor geometrical conditions. This is shown in Figure 7a for January, Figure 7b for April, Figure 7c for July and Figure 7d for October. Although the highest reflectances are observed in the backward direction along the principal plane (0°/180°),

the hot spot effect is not always well pronounced. This is partially due to the fact that the BRDF shape is retrieved from observations off the principal plane (compare Figure 4). A model specifically designed to produce a sharp hot spot effect has been proposed by *Chen and Cihlar* [1997], but we do not use it here because it introduces two additional nonlinear parameters that can only be reliably retrieved by employing observations in the vicinity of the principal plane.

4. Comparison With MODIS and MISR Albedo Products

[30] To assess the quality of the BRDF and albedo product derived by different algorithms, i.e., the PBF

Table 2. RossThick−LiSparse BRDF Parameters for the Near-Infrared Band (April 2001)

| NDVI	0.1−0.2	0.2−0.3	0.3−0.4	0.4−0.5	0.5−0.6	0.6−0.7	0.7−0.8	0.8−1.0
				Open Shrublands				
a_0	-	0.300	0.304	0.294	0.314	0.345	0.349	0.418
a_1	-	0.219	0.263	0.365	0.368	0.259	0.381	0.247
a_2	-	0.051	0.057	0.036	0.041	0.040	0.027	0.032
Error, %	-	11.03	10.52	11.01	9.87	5.25	9.16	4.67
				Grasslands				
a_0	-	0.262	0.267	0.282	0.316	0.342	0.383	0.437
a_1	-	0.184	0.264	0.294	0.265	0.173	0.209	0.350
a_2	-	0.035	0.025	0.015	0.022	0.015	0.024	0.030
Error, %	-	9.51	9.83	8.30	7.37	6.89	6.55	5.88
				Croplands				
a_0	-	0.275	0.297	0.321	0.353	0.379	0.409	0.445
a_1	-	0.165	0.123	0.166	0.167	0.183	0.241	0.238
a_2	-	0.035	0.037	0.032	0.038	0.032	0.020	0.010
Error, %	-	7.36	9.35	8.75	10.52	10.03	8.96	8.96
				Deciduous Forest				
a_0	-	-	0.252	0.260	0.283	0.315	0.357	0.395
a_1	-	-	0.127	0.081	0.066	0.074	0.115	0.099
a_2	-	-	0.049	0.042	0.053	0.054	0.076	0.114
Error, %	-	-	15.28	10.77	7.98	6.55	9.68	7.86
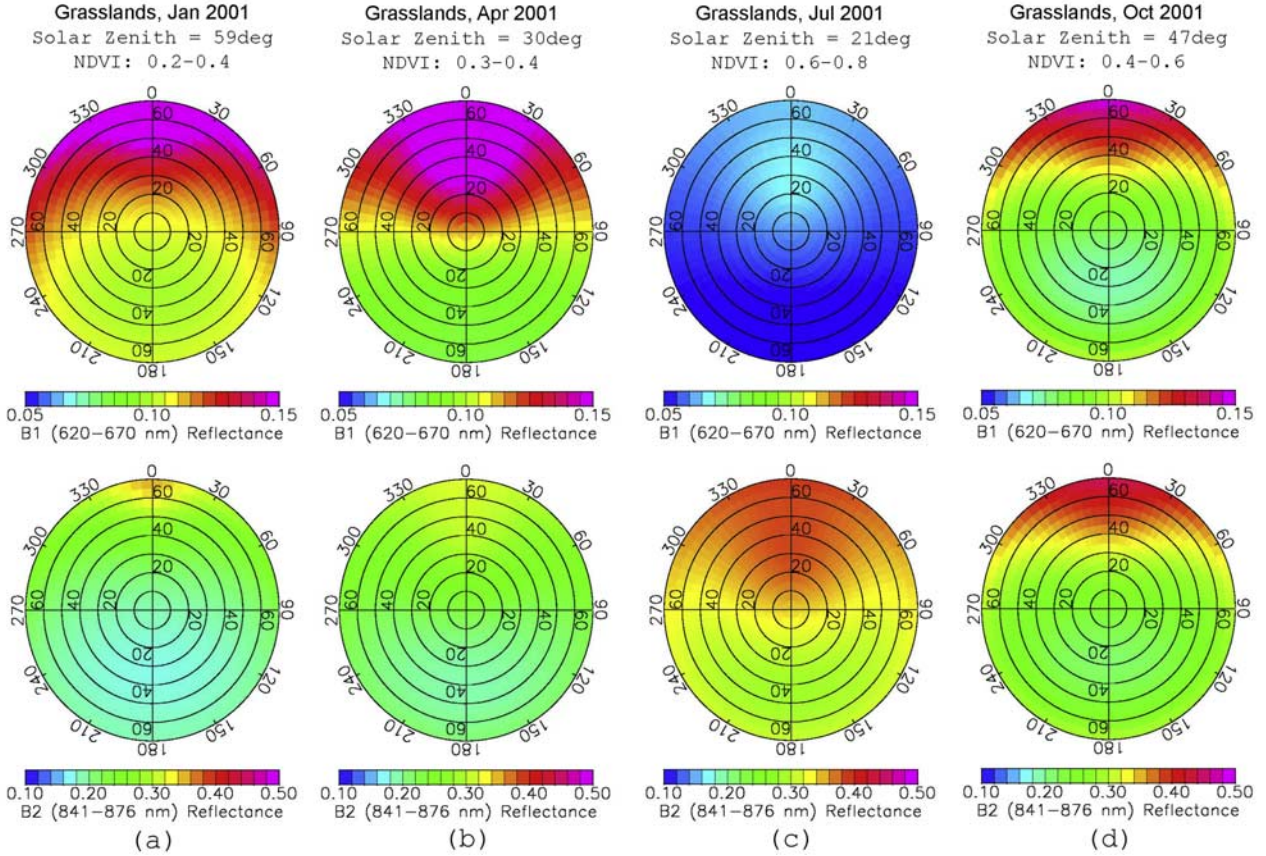
Figure 7. Polar plots of grassland surface reflectance for two spectral bands ((top) red and (bottom) NIR) from the RossThick−LiSparse BRDF model results based on the MODIS observations shown in Figure 4 for year 2001: (a) January, (b) April, (c) July, and (d) October. The SZA and the NDVI intervals are indicated at the top of each panel.

and LBF methods and approaches based on different BRDF models, we compare the LBF results described earlier to the standard MODIS albedo products (MOD43 [*Schaaf et al.*, 2002]) and the MISR surface products (D. J. Diner et al., MISR level 2 surface retrieval, Report JPL D-11401, Jet Propulsion Laboratory (JPL), 1999, available at http://eospso.gsfc.nasa.gov/eos_homepage/for_scientists/atbd/docs/MISR/atbd-misr-10.pdf, hereinafter referred to as Diner et al., 1999). The MODIS albedo products have recently been validated against ground measurements through the upscaling of fine-resolution satellite imagery such as Landsat ETM+ [*Liang et al.*, 2002] and observations from other satellite systems [*Jin et al.*, 2002, 2003b].
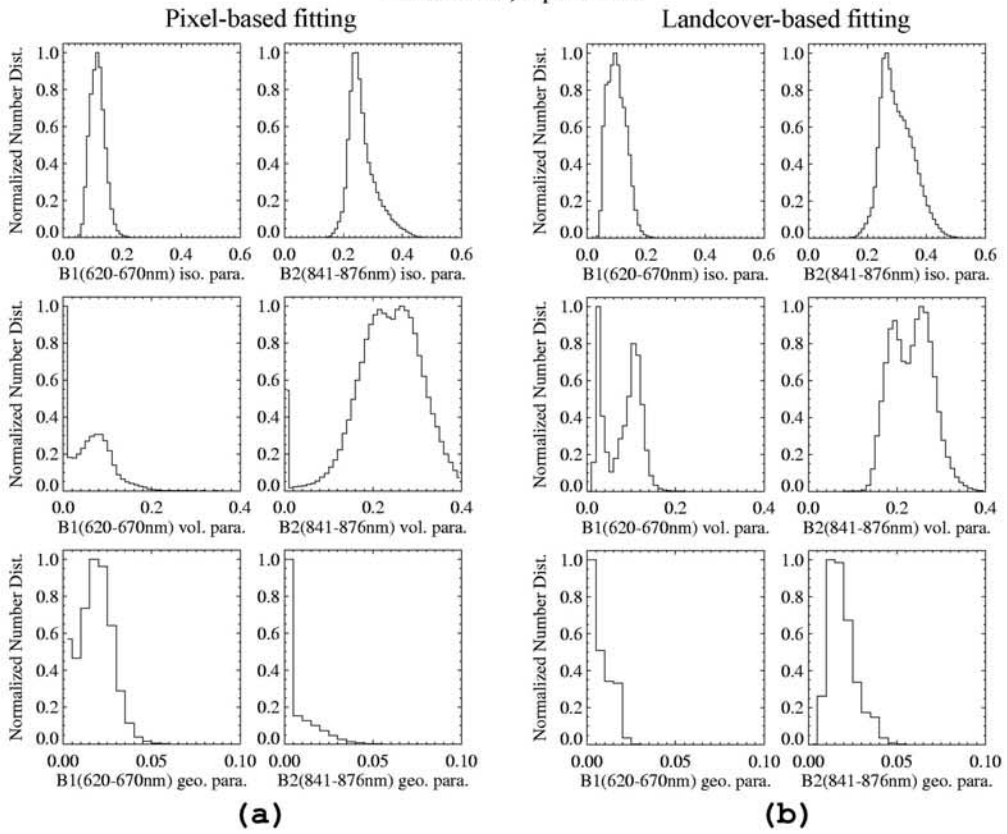
4.1. Comparison of BRDF Kernel Parameters

[31] Figures 8a and 8c show the distribution of the three kernel parameters a_0, a_1 and a_2 in the red and NIR bands from the PBF-derived MODIS 16-day albedo product (MOD43B1). Figures 8b and 8d show the same parameters but from the LBF method. All histograms in Figure 8 are normalized with peak values equal to 1. Most distributions have a single peak value. However, a number of the distributions are bimodal. This indicates that the data points for most individual land cover types are closely related, while some others, such as the grasslands, may reveal the intraclass heterogeneity. That is, they can be separated into

subclasses, for example, pasture-like grasslands and grasslands containing some portion of forest or crops fields. The large fraction of zero values for the volumetric (a_1) and geometric (a_2) parameters from the PBF retrieval indicates frequent failures of the inversion procedure [*Schaaf et al.*, 2002; *Jin et al.*, 2003a]. The LBF approach has a much higher rate of successful fitting. In general, the LBF and PBF fitting procedures show good agreement for grassland. The LBF volumetric parameter distribution is much sharper than the distribution from the MOD43 product. This is because the LBF method uses a larger number of data points for each fitting process, a shorter sampling interval of 10 days, and a higher spatial pixel resolution of 500 m. The MOD43 product has a sampling interval of 16 days and a spatial resolution of 1 km. The LBF approach is thus able to reduce intrinsic noise in its data and capture finer-resolution spatial heterogeneity.

[32] A noticeable difference between the PBF and LBF approaches occurs between the forest volumetric and geometric parameters. The PBF fails to fit the red band volumetric parameter for a significant portion of forest pixels, while the LBF successfully retrieves this parameter. Owing to its frequent inability to fit the red band volumetric parameter, the PBF approach's geometric parameter is also questionable. In the NIR band, the PBF obtains significantly larger and broader volumetric scattering and smaller geo-
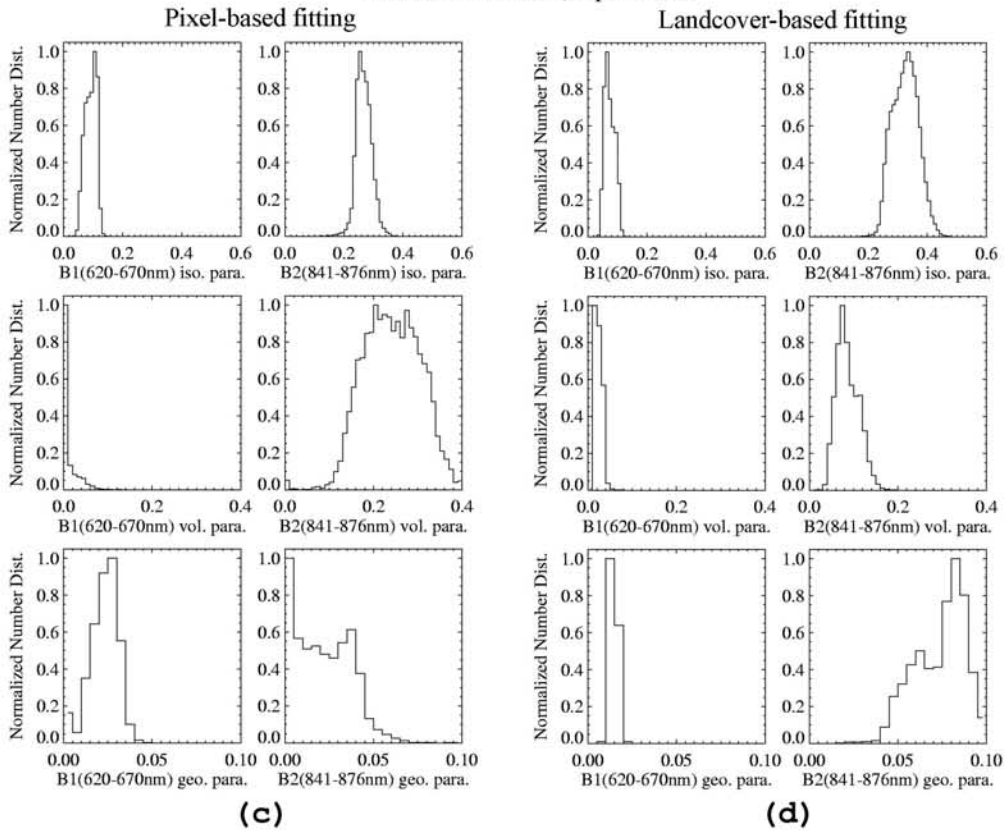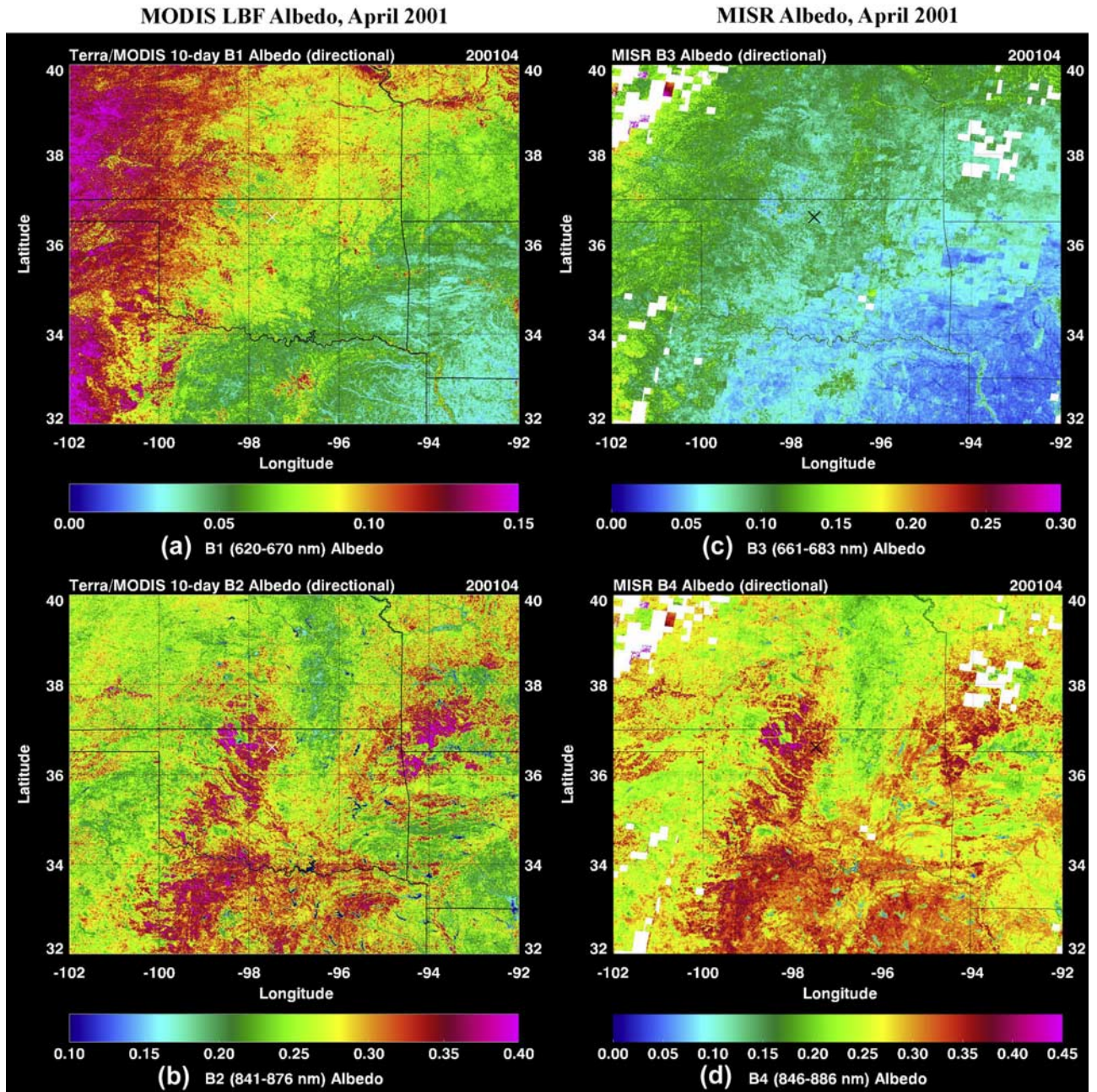
Grasslands, April 2001

Pixel-based fitting

Landcover-based fitting

(a)

(b)

Deciduous Forest, April 2001

Pixel-based fitting

Landcover-based fitting

(c)

(d)

Figure 8

MODIS LBF Albedo, April 2001

MISR Albedo, April 2001

(a) B1 (620-670 nm) Albedo

(c) B3 (661-683 nm) Albedo

(b) B2 (841-876 nm) Albedo

(d) B4 (846-886 nm) Albedo

Figure 9. Albedo images in the red and NIR bands over the ARM-SGP area. MODIS LBF albedo in bands (a) 1 (red) and (b) 2 (NIR). MISR albedo in bands (c) 3 (red) and (d) 4 (NIR). (left) Two images produced using the land cover–based fitting (LBF) algorithm. (right) Two images corresponding to the MISR L2 pixel-based albedo products. The MODIS image is an average of three 10-day interval albedo images for April 2001. The MISR image is a 1-month composite generated from days 91 to 120 (April) of 2001.

metric scattering parameters compared to the LBF approach. Considering the forest properties in the spring season, lower volumetric but higher geometric scatterings may be expected. Thus it appears that the LBF method provides more realistic results. In addition to the differences in spatial resolution, the above results may also be caused by significant temporal variations in surface properties during the 16-day sampling period. Numerous cases of fitting

Figure 8. Histograms of the three RossThick-LiSparse BRDF model parameters: (top to bottom) isotropic, volumetric, and geometric in the (left) red and (right) NIR bands in April 2001: (a) grassland, MOD43B1 (pixel-based fitting); (b) grassland, land cover–based fitting; (c) deciduous forest, MOD43B1; and (d) deciduous forest, land cover–based fitting.
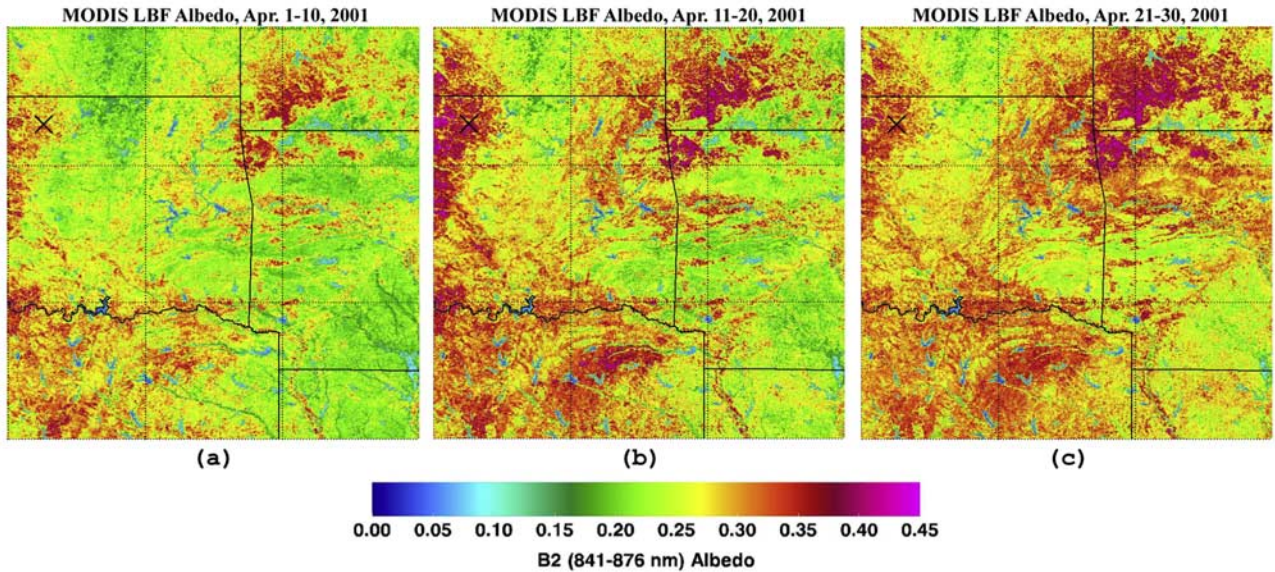
Figure 10. Albedo images in the NIR band for the southeast corner of Figure 9, derived by the MODIS LBF algorithm for 10-day intervals: (a) 1–10 April 2001, (b) 11–20 April 2001, and (c) 21–30 April 2001.

failure for the geometric parameter may lead to biases for other BRDF parameters.

4.2. Comparison of Albedo Maps

[33] Another way of assessing the agreement between the different methodologies is a direct comparison of the albedo values produced by different approaches. Figure 9 displays clear-sky albedo computed at local solar noon for the red and NIR bands over the ARM-SGP area. These images correspond to MODIS LBF albedo in bands 1 (red, Figure 9a) and 2 (NIR, Figure 9b), and to MISR albedo in bands 3 (red, Figure 9c) and 4 (NIR, Figure 9d). The LBF-derived albedo maps correspond to an average of three MODIS 10-day clear-sky albedo composites (1–10, 11–20, and 21–30 April) from 2001. The MISR-derived albedo maps correspond to a 1-month composite created by mosaicking individual MISR orbits from day 91 to 120 during 2001. These data are extracted from the MISR Level 2 Land Surface Data product, and albedo is derived using the modified Rahman's BRDF model employed in MISR data processing (Diner et al., 1999). Albedo over the white areas in Figures 9c and 9d could not be determined because of persistent cloudiness observed in MISR data within entire time interval.

[34] Figure 9 shows that the MODIS LBF and MISR produce surface albedo maps with similar spatial patterns and magnitude even though results are based on different methodologies and different sensors. However, the LBF albedo maps are much less influenced by cloud contamination and retrieval failures. This is most apparent if comparing the northwest corners of the MISR albedo images (Figures 9c and 9d). In addition, the MISR product generally produces larger albedo values than the LBF approach for the NIR band in the southern part of the study area. This phenomenon likely relates to the temporal mismatch between the MODIS LBF and MISR data points (an average of three 10-day composites versus a 1-month composite, respectively). Detailed analysis shows that the MISR albedo data in the southern part of the image are filled mostly from observations made on April 25 (a MISR compositing uses one point during a month). As a result, the noted discrepancy between data sets is caused by the rapid changes of surface vegetation properties in the spring season. This is also illustrated in Figures 10a–10c, which show three MODIS LBF 10-day NIR images for the southeastern portion of the study area (32°–38°N, 92°–98°W). These images clearly show significant changes in surface albedo in springtime. Figure 10 also reemphasizes the advantage of the LBF approach for mapping rapid changes in surface properties over short time intervals.

[35] Pixel-by-pixel comparisons between MISR and MODIS LBF albedo in the red and NIR bands are presented in Figure 11 for April 2001. Results are grouped into the five major land cover types identified in the ARM SGP area. In most cases the data points are distributed around the 1:1 line. Correlation coefficients (R) between the two data sets vary from 0.55 to 0.92 (mostly greater than 0.8). The differences in spatial resolution between MISR and MODIS images and resampling during reprojection step may contribute to scattering of the points and toward reducing the correlation coefficient. The mean bias ($\bar{\Delta}$) is also shown in Figure 11. It is an average of differences between the MISR and MODIS albedos. Positive $\bar{\Delta}$ means MISR albedo is greater than MODIS on average. Both R and $\bar{\Delta}$ are indicators of any systematic discrepancies that may exist between the two data sets. Mean biases are small. The absolute values of mean biases on Figure 11 are less than 0.01 for the red band and less than 0.037 for the NIR band. Another important parameter also shown in Figure 11 is the standard deviation (δ) of the bias. The values of δ are of magnitude around 0.01 for the red band and 0.02 for the NIR band. In general, MISR albedo is slightly larger than MODIS albedo. Such bias may be caused by many factors, such as differences in calibration, atmospheric corrections, and spectral
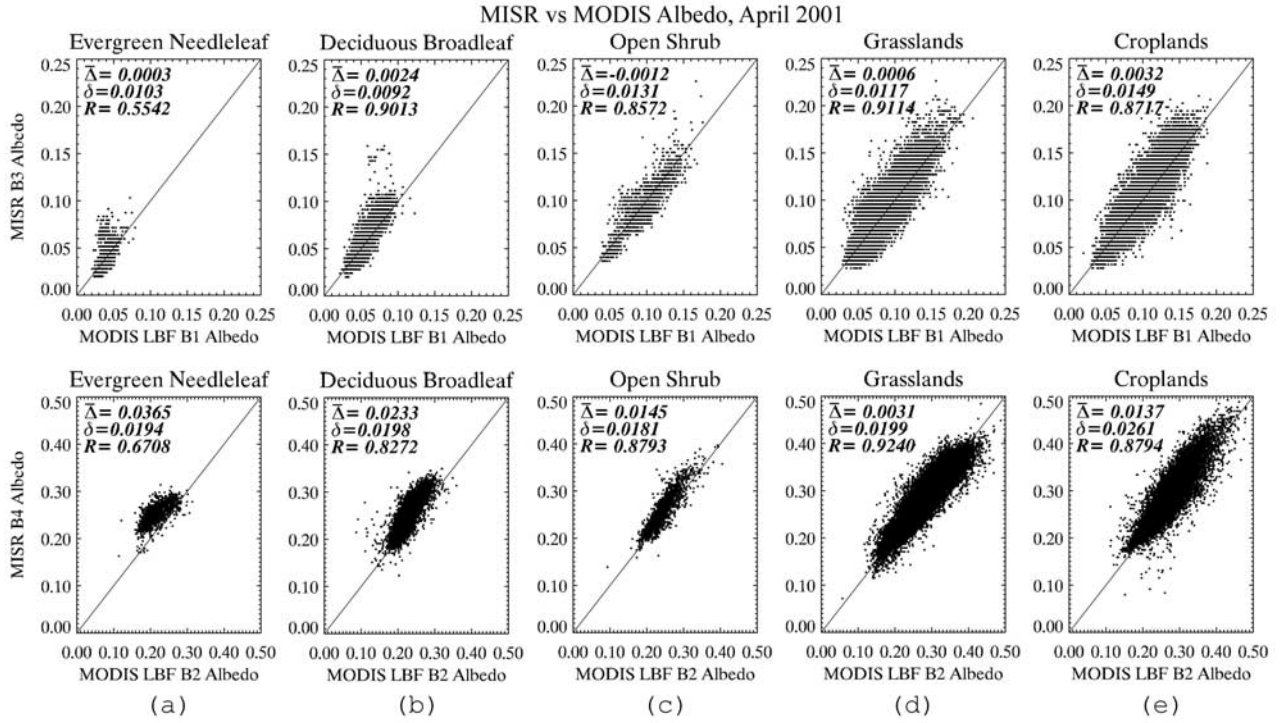
MISR vs MODIS Albedo, April 2001

Figure 11. Scatterplots of MISR albedo plotted against MODIS albedo derived by the land cover-based fitting algorithm for two spectral bands ((top) red and (bottom) NIR) for April 2001: (a) evergreen needleleaf forest, (b) deciduous broadleaf forest, (c) open shrublands, (d) grasslands, and (e) croplands.
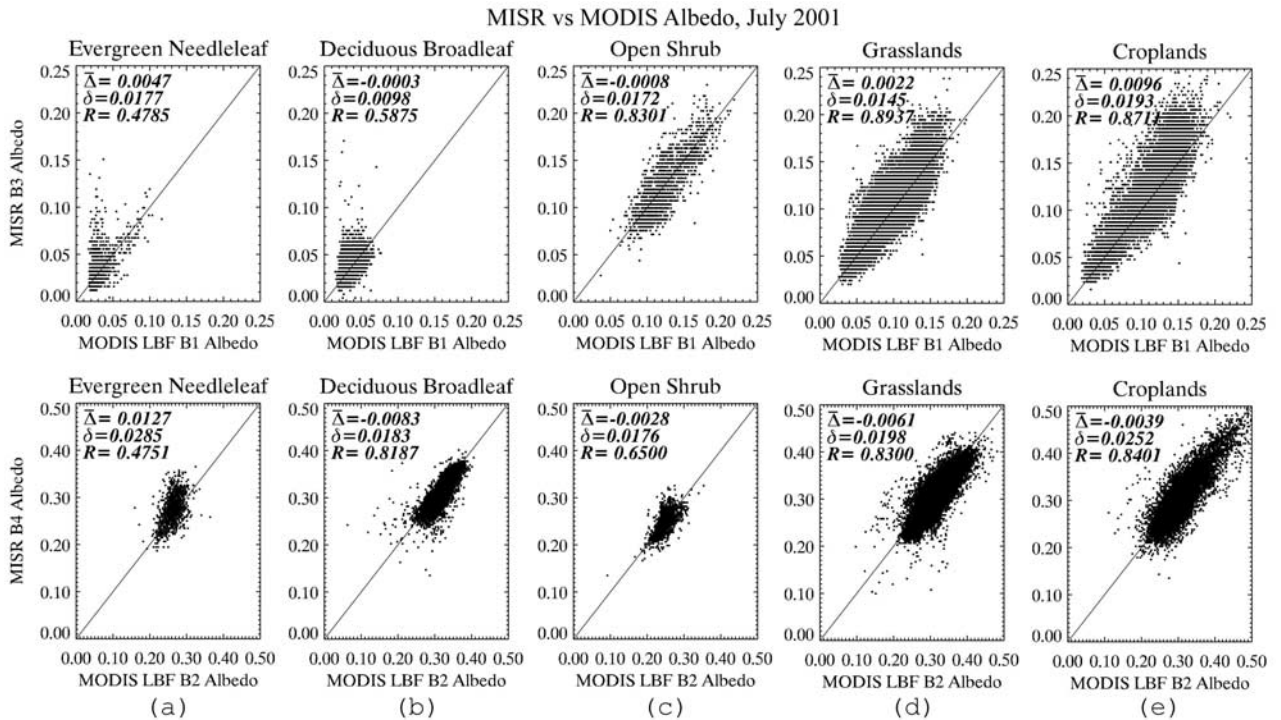
MISR vs MODIS Albedo, July 2001

Figure 12. Scatterplots of MISR albedo plotted against MODIS albedo derived by the land cover–based fitting algorithm for two spectral bands ((top) red and (bottom) NIR) for July 2001: (a) evergreen needleleaf forest, (b) deciduous broadleaf forest, (c) open shrublands, (d) grasslands, and (e) croplands.

response functions of the MODIS and MISR instruments [*Trishchenko et al.*, 2002]. This bias is also consistent with the findings of *Kahn et al.* [2004].

[36] Among all land cover types, grasslands (Figure 11d) show the best correlation between sensors, while the evergreen needleleaf forest (Figure 11a) shows less correlation. These differences can be explained, at least partially, by the difference in BRDF models used. The RossThick–LiSparse model used for MODIS data processing is more suitable to a surface covered by shorter vegetation, while the Rahman's model used in the MISR products is more accurate for taller vegetation such as forest canopies [*Privette et al.*, 1997].

[37] Pixel-by-pixel scatterplots for July 2001 are shown in Figure 12. Again, good agreement is found between MODIS LBF and MISR data sets. The best correlations are found between grasslands and croplands (Figures 12d and 12e), while the weakest correlations are found for evergreen needleleaf forest (Figure 12a). It is worth noting that a considerable number of missing and cloud contaminated pixels are present in the MISR composite albedo map for July (not shown). Cloud contamination may also partially contribute to the observed scattering of data points. When albedo comparisons include results derived for other months, a good agreement is generally found. The average biases in Figure 12 for the red and near-infrared bands are usually less than 0.01 and 0.015, the standard deviation of biases usually being less than 0.02 and the correlation coefficients typically being larger than 0.80.

5. Concluding Remarks

[38] The objectives of this work were to (1) develop a methodology suitable for retrieving surface BRDF/albedo properties from MODIS data available at 500-m spatial resolution and at 10-day time intervals; (2) overcome the difficulties in the pixel-based fitting method that are caused by using a small or insufficient number of clear-sky data points in the derivation of BRDF parameters; and (3) generate a spatially and temporally complete BRDF/albedo product over the ARM SGP area. To achieve these objectives, a land cover–based fitting (LBF) method was proposed, and applied to MODIS 500-m clear-sky directional reflectance data. Clear-sky albedo composites for 10-day intervals were derived from the MOD09A1/MYD09A1 surface reflectance product. The RossThick–LiSparse model was used to describe the shape of BRDF. A robust statistical preprocessing was implemented to provide input for the model inversion. All observations were divided into data bins according to solar zenith angle (SZA), view zenith angle (VZA) and Sun-satellite relative azimuth angle (RAA) for a given land cover type and NDVI range. A single statistical value for each data bin was produced using robust estimation. The BRDF model parameters were derived through the fitting procedure.

[39] The proposed LBF approach has several advantages. First, it increases the size of samples used in the BRDF fitting procedure, thus making the retrieval of BRDF shapes more reliable. Second, it allows the implementation of a preprocessing procedure that performs data binning, which serves to reduce noise and prevent bias caused by an uneven distribution of observational geometries. Third, it is often the only available method for producing surface BRDF/albedo products from historical data sets, which are commonly only available as a multiday clear-sky composite. Fourth, LBF-derived BRDF and albedo products may be suitable for direct applications in the studies of the regional phenological cycle and land surface modeling. Land cover–based schemes are often used to parameterize surface albedo properties in climate and GCM modeling.

[40] While the LBF approach complements the pixel-based fitting (PBF) strategy currently employed in the derivation of the MODIS standard BRDF/albedo product (MOD43), it has some advantages over the standard (PBF-derived) product. These include higher spatial resolution, shorter sampling interval, higher successful fitting rate, and capability to produce spatially complete product. It performs better and generates more realistic results when the surface vegetation state changes quickly and number of clear-sky pixels are limited because of frequent cloudiness.

[41] The methodology presented in this paper is rather general. It can be applied to other regions and data from other sensors. Because our approach is based on land cover–type sampling instead of pixel-based sampling, it can easily be applied to the data processing of multiday clear-sky composite data assembled from multiple platforms, such as Terra/MODIS, Aqua/MODIS, SPOT/VEGETATION and NOAA/AVHRR. A spectral correction procedure must be implemented to merge data from similar but not identical sensors to account for the differences in their spectral responses [*Trishchenko et al.*, 2002]. With such an approach, a more comprehensive multisatellite surface product can be generated.

[42] A good agreement between MISR-derived and LBF-derived albedo was found. Correlations between these data sets are usually larger than 0.80, and mean biases and their standard deviations are typically below 0.01 and 0.02. The distribution of model parameters derived using LBF approach also compares reasonably well with standard MOD43 product. It demonstrates more realistic features and higher success rates of model inversion.

References

Ackerman, T. P., and G. M. Stokes (2003), The atmospheric radiation measurement program, *Phys. Today*, *56*(1), 38–43.

Chen, J., and J. Cihlar (1997), A hot spot function in a simple bidirectional reflectance model for satellite applications, *J. Geophys. Res.*, *102*, 25,907–25,913.

Cihlar, J., et al. (2002), GeoComp–n, an advanced system for the processing of coarse and medium resolution satellite data. Part 2: Biophysical products for northern ecosystems, *Can. J. Remote Sens.*, *28*, 21–44.

Cihlar, J., R. Latifovic, J. Chen, A. Trishchenko, Y. Du, G. Fedosejevs, and G. Guindon (2004), Systematic corrections of the AVHRR image composites for temporal studies, *Remote Sens. Environ.*, *89*, 217–233.

Csiszar, I., G. Gutman, P. Romanov, M. Leroy, and O. Hautecoeur (2001), Using ADEOS/POLDER data to reduce angular variability of NOAA AVHRR reflectances, *Remote Sens. Environ.*, *76*, 399–409.

Diner, D. J., et al. (1998), Multi-angle Imaging SpectroRadiometer (MISR) instrument description and experiment overview, *IEEE Trans. Geosci. Remote Sens.*, *36*, 1072–1087.

Dirmeyer, P. A., and J. Shukla (1994), Albedo as a modulator of climate response to tropical deforestation, *J. Geophys. Res.*, *99*, 20,863–20,878.

Gutman, G. (1987), The derivation of vegetation indices from AVHRR data, *Int. J. Remote Sens.*, 8, 1235–1243.

Gutman, G., A. Gruber, D. Tarpley, and R. Taylor (1989), Application of angular models to AVHRR data for determination of the clear-sky planetary albedo over land surfaces, *J. Geophys. Res.*, 94, 9959–9970.

Hall, D. K., G. A. Riggs, V. V. Salomonson, N. DiGiromamo, and K. J. Bayr (2002), MODIS snow-cover products, *Remote Sens. Environ.*, 83, 181–194.

Houghton, J. T., Y. Ding, D. J. Griggs, M. Noguer, P. J. van der Linden, X. Dai, K. Maskell, and C. A. Johnson (Eds.) (2001), *Climate Change 2001: The Scientific Basis: Contribution of Working Group I to the Third Assessment Report of the Intergovernmental Panel on Climate Change*, Cambridge Univ. Press, New York.

Ingram, W. J., C. A. Wilson, and J. F. B. Mitchell (1989), Modeling climate change: An assessment of sea ice and surface albedo feedbacks, *J. Geophys. Res.*, 94, 8609–8622.

Iqball, M. (1983), *An Introduction to Solar Radiation*, 390 pp., Elsevier, New York.

Jin, Y., C. Schaaf, F. Gao, X. Li, A. Strahler, C. Bruegge, and J. Martonchik (2002), Improving MODIS surface BRDF/albedo retrieval with MISR multi-angle observations, *IEEE Trans. Geosci. Remote Sens.*, 40, 1593–1604.

Jin, Y., C. B. Schaaf, F. Gao, X. Li, A. H. Strahler, W. Lucht, and S. Liang (2003a), Consistency of MODIS surface bidirectional reflectance distribution function and albedo retrievals: 1. Algorithm performance, *J. Geophys. Res.*, 108(D5), 4158, doi:10.1029/2002JD002803.

Jin, Y., C. B. Schaaf, C. E. Woodcock, F. Gao, X. Li, A. H. Strahler, W. Lucht, and S. Liang (2003b), Consistency of MODIS surface bidirectional reflectance distribution function and albedo retrievals: 2. Validation, *J. Geophys. Res.*, 108(D5), 4159, doi:10.1029/2002JD002804.

Kahn, R., et al. (2004), MISR calibration, and implications for low-light-level aerosol retrieval over dark water, *J. Atmos. Sci.*, in press.

Knyazikhin, Y., J. V. Martonchik, R. B. Myneni, D. J. Diner, and S. W. Running (1998), Synergistic algorithm for estimating vegetation canopy leaf area index and fraction of absorbed photosynthetically active radiation from MODIS and MISR data, *J. Geophys. Res.*, 103, 32,257–32,276.

Kuusk, A. (1991), The hot spot effect in plant canopy reflectance, in *Photon-Vegetation Interactions*, edited by R. B. Myneni and J. Ross, pp. 139–158, Springer, New York.

Latifovic, R., J. Cihlar, and J. Chen (2003), A comparison of BRDF models for the normalization of satellite optical data to a standard Sun-target-sensor geometry, *IEEE Trans. Geosci. Remote Sens.*, 41, 1889–1898.

Latifovic, R., Z.-L. Zhu, J. Cihlar, C. Giri, and I. Olthof (2004), Land cover mapping of North and Central America—Global land cover 2000, *Remote Sens. Environ.*, 90, 116–127.

Li, X., and A. H. Strahler (1992), Geometric-optical bidirectional reflectance modeling of the discrete crown vegetation canopy: Effect of crown shape and mutual shadowing, *IEEE Trans. Geosci. Remote Sens.*, 30, 276–292.

Li, Z., J. Cihlar, X. Zhang, L. Moreau, and L. Hung (1996), The bidirectional effect in AVHRR measurements over boreal regions, *IEEE Trans. Geosci. Remote Sens.*, 34, 1308–1322.

Li, Z., L. Moreau, J. Cihlar, and D. W. Deering (1997), An evaluation of kernel-driven bi-directional models using PARABOLA measurements, *Can. J. Remote Sens.*, 23, 120–130.

Li, Z., M. C. Cribb, and A. P. Trishchenko (2002), Impact of surface inhomogeneity on solar radiative transfer under overcast conditions, *J. Geophys. Res.*, 107(D16), 4294, doi:10.1029/2001JD000976.

Liang, S., H. Fang, M. Chen, C. J. Shuey, C. Walthall, C. Daughtry, J. Morisette, C. Schaaf, and A. Strahler (2002), Validating MODIS land surface reflectance and albedo products: Methods and preliminary results, *Remote Sens. Environ.*, 83, 149–162.

Lucht, W., and P. Lewis (2000), Theoretical noise sensitivity of BRDF and albedo retrieval from the EOS-MODIS and MISR sensors with respect to angular sampling, *Int. J. Remote Sens.*, 21, 81–98.

Lucht, W., and J.-L. Roujean (2000), Considerations in the parametric modeling of BRDF and albedo from multiangular satellite sensor observations, *Remote Sens. Rev.*, 18, 343–379.

Lucht, W., C. B. Schaaf, and A. H. Strahler (2000), An algorithm for the retrieval of albedo from space using semiempirical BRDF models, *IEEE Trans. Geosci. Remote Sens.*, 38, 977–998.

Martonchik, J. V. (1997), Determination of aerosol optical depth and land surface directional reflectances using multi-angle imagery, *J. Geophys. Res.*, 102, 17,015–17,022.

Moody, E., M. D. King, S. Platnick, C. B. Schaaf, and F. Gao (2004), Spatially complete global surface albedos: Value-added datasets derived from Terra MODIS land products, *IEEE Trans. Geosci. Remote Sens.*, in press.

Nicodemus, F. E., J. C. Richmond, J. J. Hsia, I. Ginsberg, and T. Limperis (1977), Geometric considerations and nomenclature for reflectance, *NBS Monogr. 160*, U.S. Dep. of Commer., Washington, D. C.

Press, W. H., S. A. Teukolsky, W. T. Vetterling, and B. P. Flannery (1992), *Numerical Recipes in FORTRAN: The Art of Scientific Computing*, 2nd ed., pp. 675–683, Cambridge Univ. Press, New York.

Privette, J. L., T. F. Eck, and D. W. Deering (1997), Estimating spectral albedo and nadir reflectance through inversion of simple BRDF models with AVHRR/MODIS-like data, *J. Geophys. Res.*, 102, 29,529–29,542.

Rahman, H., B. Pinty, and M. Verstraete (1993), Coupled surface atmosphere reflectance (CSAR) model: 2. Semiempirical surface model usable with NOAA advanced very high resolution radiometer data, *J. Geophys. Res.*, 98, 20,791–20,801.

Ross, J. (1981), *The Radiation Regime and Architecture of Plant Stands*, 391 pp., Springer, New York.

Roujean, J.-L., M. Leroy, and P.-Y. Deschamps (1992), A bidirectional reflectance model of the Earth's surface for the correction of remote sensing data, *J. Geophys. Res.*, 97, 20,455–20,468.

Schaaf, C. B., et al. (2002), First operational BRDF, albedo and nadir reflectance products from MODIS, *Remote Sens. Environ.*, 83, 135–148.

Stokes, G. M., and S. Schwartz (1994), The Atmospheric Radiation Measurement (ARM) program: Programmatic background and design of cloud and radiation test bed, *Bull. Am. Meteorol. Soc.*, 75, 1201–1221.

Strugnell, N. C., W. Lucht, and C. B. Schaaf (2001), A global albedo data set derived from AVHRR data for use in climate simulations, *Geophys. Res. Lett.*, 28, 191–194.

Trishchenko, A. P. (2002), Removing unwanted fluctuations in the AVHRR thermal calibration data using robust techniques, *J. Atmos. Oceanic Technol.*, 19, 1939–1954.

Trishchenko, A. P. (2004), Concept of a new multiangular satellite mission for improved bidirectional sampling of surface and atmosphere properties, in *Earth Observing Systems IX*, edited by W. L. Barnes and J. J. Butler, *Proc. SPIE Int. Soc. Opt. Eng.*, 5542, 97–108.

Trishchenko, A. P., J. Cihlar, and Z. Li (2002), Effects of spectral response function on the surface reflectance and NDVI measured with moderate resolution sensors, *Remote Sens. Environ.*, 81, 1–18.

Trishchenko, A. P., K. Khlopenkov, and Y. Luo (2004), Retrieval of BRDF for pure landcover types from MODIS and MISR using an angular unmixing approach, in *Weather and Environmental Satellites*, edited by T. H. Vonder Haar and H.-L. A. Huang, *Proc. SPIE Int. Soc. Opt. Eng.*, 5549, 167–175.

Wanner, W., X. Li, and A. H. Strahler (1995), On the derivation of kernels for kernel-driven models of bidirectional reflectance, *J. Geophys. Res.*, 100, 21,077–21,090.

Wanner, W., A. H. Strahler, B. Hu, P. Lewis, J.-P. Muller, X. Li, C. B. Schaaf, and M. J. Barnsley (1997), Global retrieval of bidirectional reflectance and albedo over land from EOS MODIS and MISR data: Theory and algorithm, *J. Geophys. Res.*, 102, 17,143–17,161.

Wu, A., Z. Li, and J. Cihlar (1995), Effects of land cover type and greenness on advanced very high resolution radiometer bidirectional reflectances: Analysis and removal, *J. Geophys. Res.*, 100, 9179–9192.

———————————

R. Latifovic and A. P. Trishchenko, Canada Centre for Remote Sensing, Earth Sciences Sector, Natural Resources Canada, 588 Booth Street, Ottawa, Ontario, Canada K1A0Y7. (trichtch@ccrs.nrcan.gc.ca)

Y. Luo, Noetix Research, Inc., 403-265 Carling Avenue, Ottawa, Ontario, Canada K1S 2E1.

Z. Li, Department of Meteorology and Earth System Science Interdisciplinary Center, University of Maryland, College Park, MD 20742, USA.